Journal of Renewable Materials

Tech Science Press

DOI: 10.32604/jrm.2023.027512

ARTICLE

Study on Mechanical Properties of High Fine Silty Basalt Fiber Shotcrete Based on Orthogonal Design

Jinxing Wang[1,2,3], Yingjie Yang[1,2,3], Xiaolin Yang[1,2,3], Huazhe Jiao[1,2,3,4,*], Qi Wang[1,2,3], Liuhua Yang[1,2,3], Jianxin Yu[1,2,3] and Fengbin Chen[1,2,3]

[1]State Collaborative Innovation Center of Coal Work Safety and Clean-Efficiency Utilization, School of Civil Engineering, Henan Polytechnic University, Jiaozuo, 454003, China

[2]Provincial Key Laboratory of Underground Engineering and Disaster Prevention and Control, School of Civil Engineering, Henan Polytechnic University, Jiaozuo, 454003, China

[3]School of Civil Engineering, Henan Polytechnic University, Jiaozuo, 454003, China

[4]Key Laboratory of Mine Ecological Effects and Systematic Restoration, Ministry of Natural Resources, Beijing, 100081, China

[*]Corresponding Author: Huazhe Jiao. Email: jiaohuazhe@hpu.edu.cn

Received: 02 November 2022 Accepted: 13 January 2023 Published: 26 June 2023

ABSTRACT

In order to improve the comprehensive utilization rate of high fines sand (HFS) produced by the mine, full solid waste shotcrete (HFS-BFRS) was prepared with HFS as fine aggregate in cooperation with basalt fiber (BF). The strength growth characteristics of HFS-BFRS were analyzed. And the fitting equation of compressive strength growth characteristics of HFS-BFRS under the synergistic effect of multiple factors was given. And based on the orthogonal experimental method, the effects on the compressive strength, splitting tensile strength and flexural strength of HFS-BFRS under the action of different levels of influencing factors were investigated. The effect of three factors on the mechanical properties of HFS-BFRS, 3, and 28 d, respectively, was revealed by choosing the colloidal sand ratio (C/H), basalt fiber volume fraction (BF Vol) and naphthalene high-efficiency water reducing agent (FDN) as the design variables, combined with indoor tests and theoretical analysis. The results show that the sensitivity of the three factors on compressive strength and flexural strength is C/H > FDN > BF Vol, and splitting tensile strength is BF Vol > FDN > C/H. Finally, the fitting ratio of HFS-BFRS was optimized by the factor index method, and the rationality was verified by the field test. For the fluidity of HFS-BFRS, the slump can be improved by 139% under the action of 1.2% FDN, which guarantees the pump-ability of HFS-BFRS.

KEYWORDS

Solid wastes recycling; high-fine silt; basalt fiber; total solid waste shotcrete; orthogonal design

Nomenclature

HFS	High-fine silt
FDN	Naphthalene high-efficiency water-reducing agent
BF	Basalt fiber

1 Introduction

With the rapid development of China's infrastructure construction and the strengthening of environmental protection, natural sand resources are gradually in shortage, and to meet the increasing demand for engineering construction, the rock is often mined and mechanically crushed to produce mechanism sand (MS). Compared with natural sand, the production process of MS inevitably produces stone powder with a particle size of less than 75 μm and the same lithology as the parent rock, and its excessive content will affect the cracking resistance and mechanical properties of concrete with MS as fine aggregate, and reduce the durability of concrete [1]. Wind sorting, vibratory screening, and water washing are commonly used in engineering to deal with excessive stone powder [2]. However, this is not only detrimental to the full utilization of MS but also raises its production cost, as well as has many negative impacts on sand resources and environmental protection. Therefore, how to resourcefully utilize high fines sand (HFS) has become a hot topic of concern in the industry.

China Henan Jiaozuo Qianye New Material Co., Ltd. produces a large amount of high fine silt (HFS) in the aggregate production process, with an annual output of about 4 million to 5 million tons. The production process is shown in Fig. 1. Compared with ordinary mechanism sand, the most significant feature of HFS is the relatively high content of fines (mainly limestone powder) with particle size less than 75 μm, which is in the range of 20% to 25%, and poor particle size and unstable mud content. Due to the lack of an in-depth theoretical basis or suitable market conditions, its resource utilization has become a major technical problem, but the large amount of work accumulated in the early stage has also laid an important foundation for the further depth of this study.

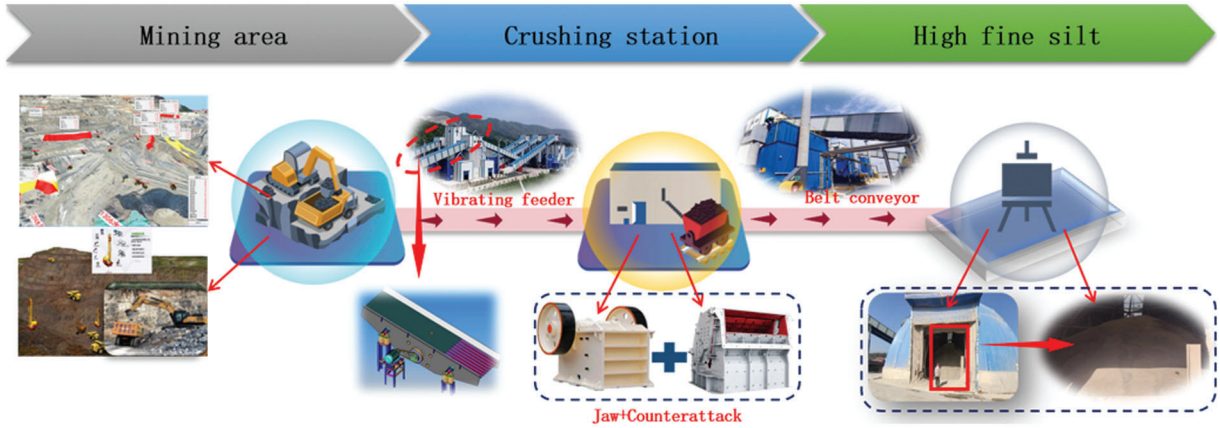

Figure 1: Production process of high fine silt

Many scholars at home and abroad have studied the effect of stone powder on concrete properties, and when the stone powder is applied to different types of concrete, its optimal admixture rate has significant differences. Rayed et al. [3] found that the compressive strength was increased from 30 to 41 Mpa when stone powder replaced cementitious materials at a replacement rate of 20%. The physical filling effect of stone powder on the concrete matrix [4] helps to improve the particle packing density of HFS, and the tiny particles are filled in the aggregate gaps as micro-aggregates [5–7], and the strength is improved. At the same time, the friction between the solid particles increases, resulting in an increase in yield stress, plastic viscosity, and thixotropy of the concrete, resulting in a decrease in the concrete slump. Westerholm et al. [8] showed that for cement slurry without HFS, the yield stress and plastic viscosity increased by 125%, 500%, and 100%, 500%, respectively, as the limestone rock flour admixture increased from 13.3% to 26.1%. and 100%, 500%. Schmidt et al. [9] and Moir et al. [10] observed that

the stone powder's morphological effect and filler effect was not favorable for the development of concrete compatibility when the stone powder content exceeded 20%. In addition, Aliabdo et al. [11] and Rodrigues et al. [12] found through their studies that the tensile strength and modulus of elasticity of concrete mixed with high content of stone dust were generally reduced. However, the incorporation of fibers can significantly improve fine aggregate concrete's tensile strength, crack resistance, and ductility.

With its excellent mechanical properties and environmentally friendly manufacturing process, basalt fiber (BF) is widely used in the field of concrete reinforcement [13–16]. After the incorporation of BF in concrete, a significant yield point in the stress-strain curve appears, and BF at less than 0.3% admixture contributes to the growth of tensile and compressive strength of concrete [17]. SIM [18] showed that BFRC, compared with ordinary concrete, has a high tensile strength of 0.5 to 1.0 times and 3 to 5 times higher elongation. Dias et al. [19] investigated the relationship between BF/concrete fracture toughness and fiber admixture, and the experimental results showed that the ultimate load and ultimate deformation of BF/concrete beams before damage were substantially increased, and the sensitivity to cracking was reduced. Jiao et al. [20] found the effect law of basalt fibers on the toughness of shotcrete with the help of microscopic scanning and obtained the optimum fiber content. At the same time, the network structure formed by the three-dimensional disordered distribution of fibers in the concrete matrix produced a bonding effect, which led to the secondary strengthening of the matrix and reduced the shotcrete resilience.

The orthogonal test is a multi-factor and multi-level experimental design method that can reduce the required tests and optimize the mix ratio to ensure representative test results [21]. Aiming at the raw material system of Qianye's new material, shotcrete was prepared by using total solid waste aggregate and basalt fiber. Orthogonal experiments studied the mechanical properties of HFS-BFRS with the binder-aggregate ratio (C/H), the volume fraction of basalt fiber (BF), and the content of Naphthalene high-efficiency water-reducing agent (FDN) as factors.

2 Materials and Methods

2.1 Materials

The test cement is P.O42.5 ordinary silicate cement, and the performance index meets the requirements of General Silicate Cement (GB 175-2007). The water the reducing agent is naphthalene, high efficient water-reducing agent, powder, see Fig. 2a. The water reduction rate is 17%. The quick-setting agent is an alkali-free powder quick-setting agent, as is shown in Fig. 2b tested. The initial setting of cement net paste mixed with the quick-setting agent is 2∼3 min, and the final setting is 8∼10 min.

(a) FDN (b) No alkali accelerating (c) Basalt fiber

Figure 2: Raw materials for the test

The fiber is 18 mm short-cut BF. See Fig. 2c. Its physicochemical parameters are shown in Table 1. the fine aggregate is high-fine powder sand produced by Qianye New Material, and the fine powder content is

22.2%, composed of stone powder and mud powder. The chemical composition of both is shown in Table 2. The fibers and limestone powder were scanned using the JSM-6390LV SEM introduced by Nippon Electron Corporation, and the results are shown in Fig. 3.

Table 1: Performance parameters of basalt fiber (BF)

Fibre	Length/ (mm)	Diameter/ (μm)	Density/ $g \cdot cm^{-3}$	Tensile strength/ (MPa)	Elastic modulus/ (GPa)	Elongation at break (%)
BF	18	13	2.65	4100–4800	80–100	2.7–3.4

Table 2: Chemical composition of stone powder and bentonite (%)

Materials	SiO_2	Al_2O_3	Fe_2O_3	CaO	MgO	Na_2O	K_2O	P_2O_5	SO_3	Loss
Powder	0.32	/	0.20	53.65	4.25	/	/	/	/	41.59
Bentonite	69.50	13.15	2.63	1.36	2.14	1.68	2.10	0.17	0.056	7.21

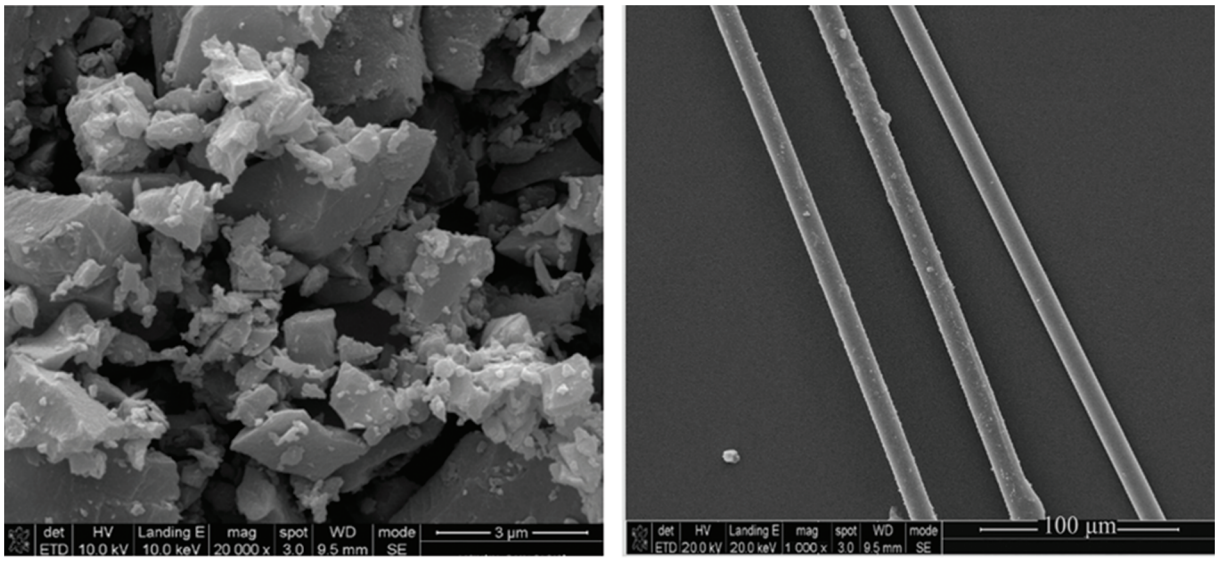

(a) Limestone powder (b) Basalt fibers

Figure 3: Micro photos of stone powder and fiber morphology

From the SEM image, the stone powder particles are of different sizes, and many small particles adhere to the large particles and are not completely dispersed. The surface morphology of the particles is angular and irregular geometry, and the texture is hard with a clear mineral deconstruction surface. The surface of basalt fiber is smooth overall, but there are defects such as bumps and scratches and stress concentrations may occur at these locations.

The coarse aggregate of shotcrete accounts for a large proportion, which is prone to shrink and crack, thus affecting the strength [22]. Compared with ordinary shotcrete, fine aggregate shotcrete has comprehensive advantages such as low cost, good heat insulation, and durability [23,24]. HFS-related physical performance indexes are shown in Table 3, its MB value is detected in Fig. 4, its particle size distribution is measured in Table 4, and the fluctuation curve of fineness modulus is shown in Fig. 5.

Table 3: Fine aggregate parameters

Aggregate	Fineness modulus	Apparent density/(kg·m^{-3})	Loose bulk density/(kg·m^{-3})	Compact bulk density/(kg·m^{-3})	Moisture content/%	Powder content/%
HFS	2.98	2573	1647.4	2023.2	1.81%	20.3%

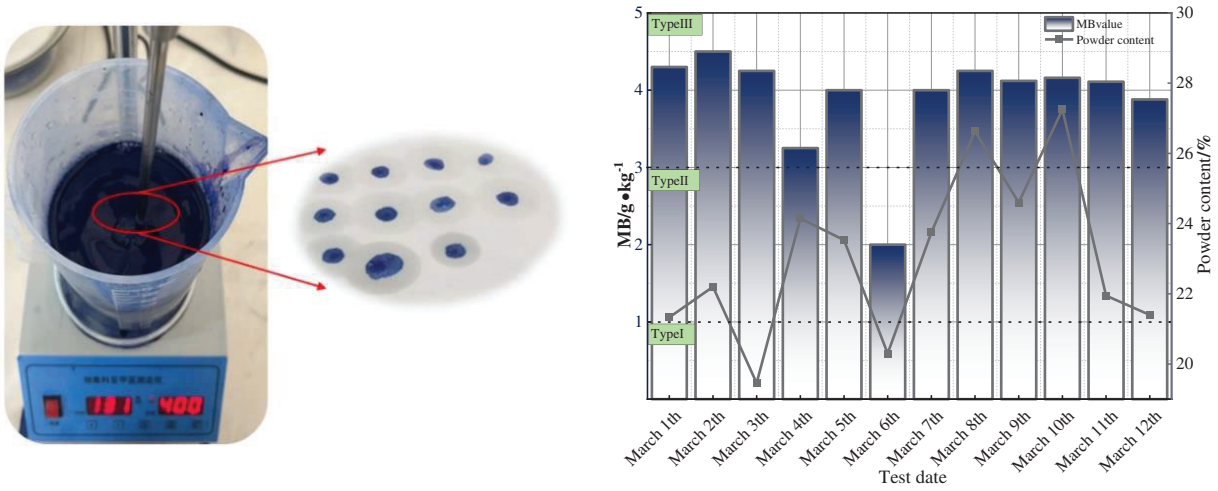

(a) Methylene blue adsorption test

(b) Change trend of MB value and powder content

Figure 4: Detection of powder content and MB value

Table 4: HFS particle size distribution

Particle size/mm	Mass/g	Grader retained percentage/%	Accumulated retained percentage/%
>4.75	4.9	1.0	1.0
2.36~4.75	100.0	20.6	21.6
1.18~2.36	94.9	19.5	41.1
0.6~1.18	72.5	14.9	56.0
0.3~0.6	71.3	14.7	70.6
0.15~0.3	28.1	5.8	76.4
Sieve bottom	114.7	23.6	100.0

2.2 Analysis of HFS-BFRS Strength Growth Characteristics

Through the exploratory test carried out in the early stage, the influence trend of water-binder ratio and quick-setting agent on the compressive strength of shotcrete test block with high-fine silt was obtained through comprehensive analysis, as shown in Fig. 6.

It can be seen from Fig. 6 that the compressive strength is negatively correlated with the water-binder ratio, and the compressive strength decreases by 17.8% in 28 d. The high water-binder ratio leads to the migration of free water in the mixture under the action of pore pressure, resulting in the formation of tiny capillary pores, increasing the internal porosity, and then the strength decreases. In addition, with the increase of quick-setting agent dosing, the 28 d compressive strength showed a gradually decreasing

trend, and the decreasing trend was gradually slowed down with the increase of quick-setting agent dosing, and the 28 d compressive strength decreased by 13%. This is because the intervention of a quick-setting agent destroys the original setting process of the system and accelerates the hydration of C_3A in the early stage, while the normal situation should be C_3S hydration to generate early strength, aluminate hydration products compared to silicate hydration products there is a certain instability, the subsequent process may cause crystal transformation, resulting in the appearance of pore holes, affecting the strength. At the same time, the aluminate hydration products formed too quickly in the early hydration are wrapped around the cement, inhibiting further hydration, which in turn leads to late strength decay.

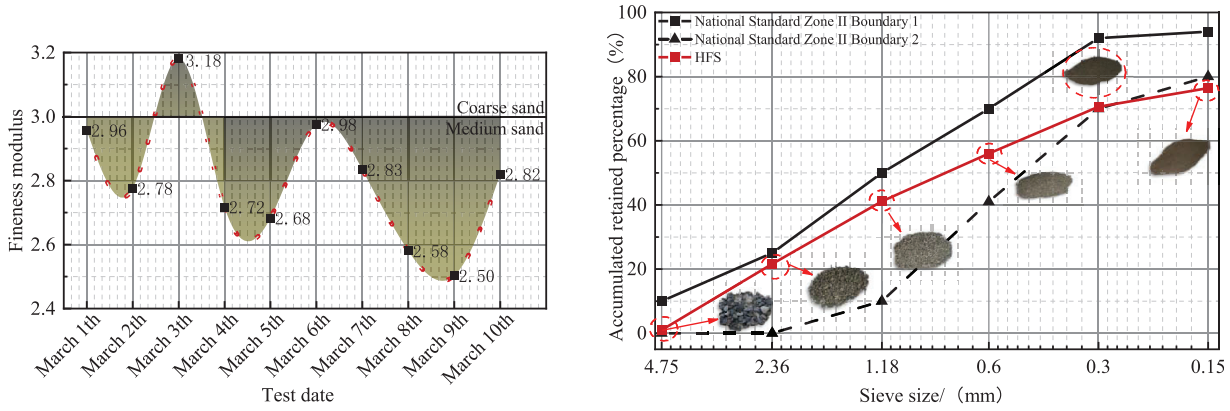

(a) Change trend of HFS fineness modulus (b) HFS particle size

Figure 5: HFS fineness modulus

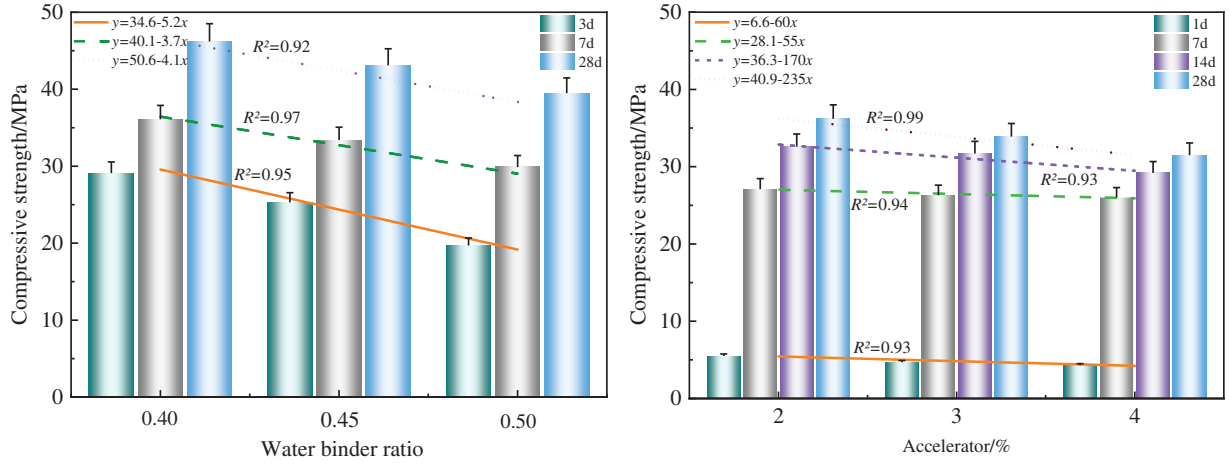

Figure 6: Relationship between water-binder ratio, accelerating agent, and compressive strength

For the 1% admixture of the quick-setting agent, its initial setting time is 8.3 min and the final setting time is 15.5 min, which does not meet the requirements of the standard (GB/T35159-2017). Considering the actual effect and economic benefits, the 2% dose was selected in the subsequent orthogonal test.

Li et al. [25] found that the compressive strength of shotcrete mixed with a quick-setting agent meets the Eq. (1):

$$\sigma_{c,t} = \sigma_{c,0}(1 - e^{-\alpha t}) \tag{1}$$

where: $\sigma_{c,t}$ is compressive strength, MPa; $\sigma_{c,0}$ is final compressive strength, MPa; α is time constants.

To study the strength growth law of HFS-BFRS with different quick-setting agent admixtures, the 1, 7, 14, and 28 d compressive strengths were counted using quick-setting agent admixtures of 2%, 3%, and 4%. The data were fitted using Eq. (1), and the fitted curves are shown in Fig. 7.

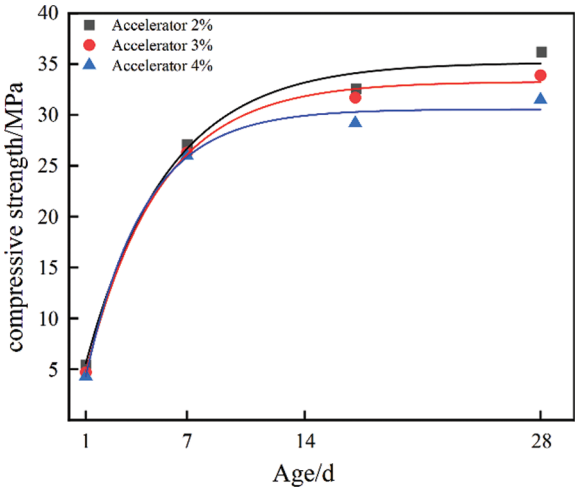

Figure 7: Effect of age on the development of compressive strength

As seen in Fig. 7, when using Eq. (1) for fitting, the compressive strength grows faster at the initial stage, and the decreasing trend of the growth rate is obvious with age. The addition of a quick-setting agent greatly improves the early strength of HFS-BFRS. With increasing age, the strength continues to grow, but the decreasing growth rate trend is significant. It can be seen that Eq. (1) can better respond to the strong growth law of HFS-BFRS mixed with a quick-setting agent.

2.3 Strength Growth Characteristics of HFS-BFRS under the Action of Comprehensive Factors

Through the study of the three variables of water binder ratio, quick-setting agent admixture, and age on the compressive strength law of HFS-BFRS, it is concluded that the compressive strength of HFS-BFRS is linearly related to water-cement ratio and quick-setting agent admixture, and exponentially related to age. The final compressive strength prediction model of HFS-BFRS under the three factors was derived in the form of Eqs. (2)–(4).

$$f'_{cu,k} = \alpha_1 C + \alpha_2 \tag{2}$$

where: α_1, α_2 is the coefficient to be determined, and C is the water binder ratio.

$$f'_{cu,k} = \alpha_3 D + \alpha_4 \tag{3}$$

where: α_3, α_4 is the coefficient to be determined, D is quick-setting agent admixture, %.

$$f'_{cu,k} = \alpha_5 - (1 - e^{-\alpha_6 t}) \tag{4}$$

where: α_5, α_6 is the coefficient to be determined, t is age, d.

The influence of quick-setting agent dosage on compressive strength is greatly affected by age, so the quick-setting agent dosage at the same age is considered as a comprehensive effect when fitting the prediction model. The prediction model of HFS-BFRS compressive strength can be expressed as:

$$f'_{cu,k} = \beta_1 C + \beta_2 + (\beta_3 D + \beta_4) \times [\beta_5 - (1 - e^{-\beta_6 t})] \tag{5}$$

where: β_1, β_2, $\cdots$, β_6 is the model undetermined coefficient.

The regression curve is obtained by fitting the experimental data with 1stopt software, and the correlation coefficient is 0.967. See Table 5 for model regression parameters.

Table 5: Regression parameters of the compressive strength prediction model

Regression parameter	β_1	β_2	β_3	β_4	β_5	β_6
Estimated results	−4.16	39.15	−138.3	32.5	32.7	0.24
Correlation coefficient			0.967			

By introducing the undetermined coefficient of the model into Eq. (5), the fitting equation of HFS-BFRS compressive strength growth characteristics is obtained as follows:

$$f'_{cu,k} = -4.16C + 39.15 + (-138.3D + 32.5) \times [32.7 - (1 - e^{-0.24t})] \tag{6}$$

2.4 HFS-BFRS Liquidity Analysis

The moderate amount of stone powder in HFS can increase the fluidity of concrete, and the mechanism of action is expressed as the distribution of stone powder as small particles in the voids between coarse aggregates [26], making it easier for the aggregates to move freely among themselves, i.e., stone powder plays a lubricating role. However, when the stone powder content exceeds 20%, the adsorption of stone powder on the water will reduce free water in the slurry, thus limiting the fluidity of the slurry. Different stone powder contents classify the slurry into three forms, as shown in Fig. 8, the states of cement and fine powder particles in three forms are a. Cement and fine powder particles suspended in water; b. Pores between cement and fine powder particles filled with water; c. Pores between cement and fine powder particles are filled with less water [27]. The porosity between the particles in the slurry can be calculated using Eq. (7), which applies to both forms of a and b.

$$\varepsilon = \frac{m_W}{\rho_W} \Big/ \frac{m_W + m_C + m_F}{\rho} \tag{7}$$

where: ε is the porosity of slurry particles; m_F is the weight of fine powder, unit Kg; ρ is the density of slurry in Kg/m³.

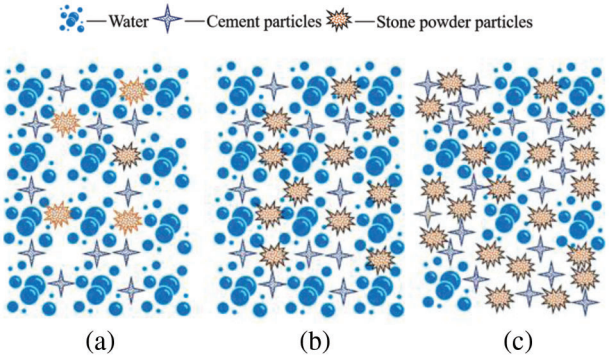

Figure 8: Physical model of slurry

In addition, the incorporation of basalt fibers increases the viscosity of HFS-BFRS, and a large amount of water and cement is adsorbed on the surface of basalt fibers. At the same time, the mesh structure formed by basalt fibers increased the cohesion of concrete and limited the fluidity and plastic deformation of concrete.

It can be seen that the stone powder (SP) and BF in HFS-BFRS harm the fluidity of HFS-BFRS, while FDN can disperse cement particles by virtue of its comb-like structure through the static repulsion effect, which occurs due to the adsorption of the particle surface or through the spatial site resistance caused by the extension of graft chains from the cement particle surface. For the optimization effect of FDN, this study compared the effect of FDN on the slump of HFS-BFRS at different contents of stone powder with 0% and 1.2% dosing of FDN.

As shown in Fig. 9, the slump of HFS-BFRS with 0% FDN admixture reaches the maximum at about 21% of stone powder content, at which time the slump is 61 mm, and according to the Technical Regulations for Shotcrete Application JGJ/T372-2016, the slump of shotcrete is easy to maintain within 80~120 mm, which is seen to be unable to meet the requirements of spraying. While for HFS-BFRS mixed with 1.2% FDN, the slump is 95 mm at this time, and the slump is improved by 56%. Compared with the slurry without FDN, the addition of FDN significantly improved the fluidity of HFS-BFRS, and the slump could be increased by up to 139%.

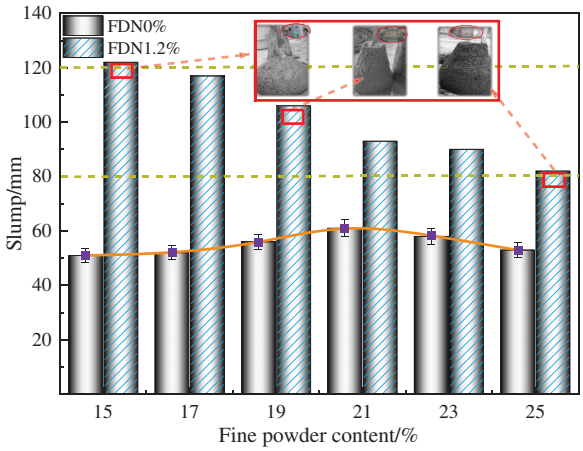

Figure 9: Relationship diagram of FDN, stone powder, and slump

Meanwhile, with the increase of stone powder content, the optimization effect of FDN on slump gradually decreases, because the electrostatic repulsive ability of FDN weakens with the increase of stone powder, and the side chain density of FDN decreases, leading to the weakening of its spatial site resistance.

2.5 HFS-BFRS Production Process

The incorporation method of fibers affects the dispersion of fibers in the concrete. A reasonable incorporation method can make the fiber better dispersed in the concrete and reduce the mixing time [28]. The mainstream fiber incorporation methods are the fiber wrapping method and secondary mixing method, Li et al. [29] compared the effect of the two incorporation methods on the compressive strength and damage of concrete, the mechanical properties of concrete using fiber wrapping method is better than those of secondary mixing method. Therefore, the fiber wrapping method was used in this study, and the test block preparation process is shown in Fig. 10.

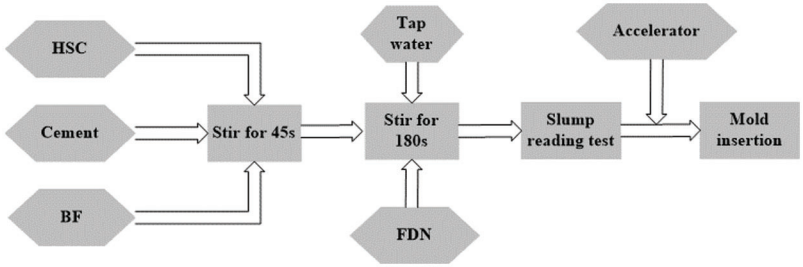

Figure 10: Test flow chart

2.6 Orthogonal Experimental Design

Taking C/H, BF, and FDN as factors, the effects of the three factors on the mechanical properties of concrete were compared to find out the optimal mix ratio. The orthogonal table L9(3^3) was used to arrange the test. The specific factors and levels were shown in Table 6, and the test combination scheme was shown in Table 7.

Table 6: Influencing factors and levels of orthogonal experiments

Levels	Factors		
	C/H	BF Vol/%	FDN/%
1	0.28	0.05	1.0
2	0.25	0.10	1.2
3	0.22	0.15	1.5

Table 7: Orthogonal test combination scheme

Code	Cement/kg	HFS/kg	Water/kg	BF/g	FDN/g	Accelerator/g
$H_{0.28}B_{0.05}F_{1.0}$	5.28	18.50	2.64	15.9	52.80	105.6
$H_{0.28}B_{0.10}F_{1.2}$	5.28	18.50	2.64	31.8	63.36	105.6
$H_{0.28}B_{0.15}F_{1.5}$	5.28	18.50	2.64	47.7	79.20	105.6
$H_{0.25}B_{0.05}F_{1.2}$	5.28	21.12	2.64	15.9	63.36	105.6
$H_{0.25}B_{0.10}F_{1.5}$	5.28	21.12	2.64	31.8	79.20	105.6
$H_{0.25}B_{0.15}F_{1.0}$	5.28	21.12	2.64	47.7	52.80	105.6
$H_{0.22}B_{0.05}F_{1.5}$	5.28	23.76	2.64	15.9	79.20	105.6
$H_{0.22}B_{0.10}F_{1.0}$	5.28	23.76	2.64	31.8	52.80	105.6
$H_{0.22}B_{0.15}F_{1.2}$	5.28	23.76	2.64	47.7	63.36	105.6

Notes: The dosage of the accelerating agent is 2% of cementing material, and BF is selected by volume fraction, 0.05% (mass 1.35 kg/m³), 0.1% (mass 2.7 kg/m³), 0.15% (mass 4.07 kg/m³), respectively, and the length is 12 mm. H-cement/sand ratio (C/H0.28, 0.25, 0.22); HFS-high-fine silt; Bf-basalt fiber; FDN-naphthalene-based high-efficiency water reducing agent.

3 Results and Discussion

3.1 Failure Forms of Specimens and Analysis of Experimental Data

The strength of concrete specimens was tested after curing for 3 and 28 d under standard curing conditions. The cube's uniaxial compressive, splitting tensile, and flexural strength loading rates were 0.5,

0.05, and 0.05 MPa/s, respectively. The dimensions of the specimen and the mechanical test model are shown in Fig. 11. The test results of non-standard specimens were converted according to Eqs. (8)–(10).

$$f_{cu} = 0.95 \times \frac{F}{A_1} \tag{8}$$

$$f_{cf} = \frac{Fl}{bh^2} \tag{9}$$

$$f_{ts} = 0.85 \times \frac{2F}{\pi A_2} = 0.541 \times \frac{F}{A_2} \tag{10}$$

where: f_{cu}, f_{cf}, f_{ts} is compressive strength, flexural strength, splitting tensile strength, unit (MPa); F is the failure load of the specimen (unit: N); A_1 is the contact surface area of the specimen; A_2 is the failure surface area of the specimen; l, b and h are the spacing, width, and height of the two points of the specimen, respectively (unit: mm). 0.95 and 0.85 are the size conversion coefficients of non-standard specimens, respectively.

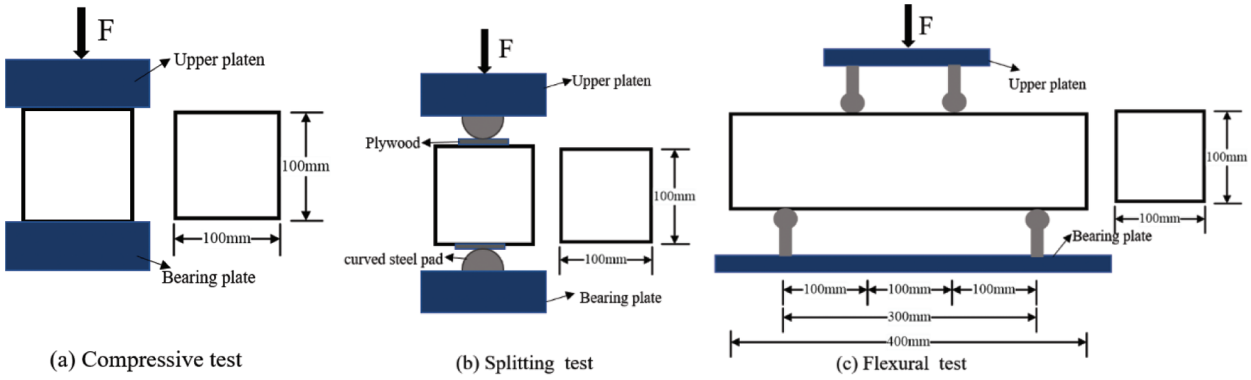

Figure 11: Mechanical test

During the destruction of the HFS-BFRS specimen, several cracks appeared along the side of the specimen through the upper and lower surfaces of the specimen, and the fibers were in full contact with the shotcrete. The enhanced surface adhesion effectively prevented the direct spalling of concrete fragments and still showed good integrity after the damage. The damage pattern of the specimen block is shown in Fig. 12.

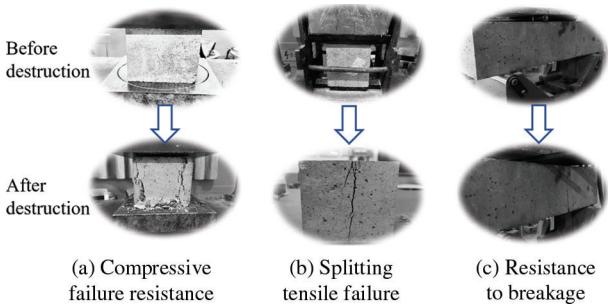

Figure 12: Failure diagram of a specimen

Uniformly distributed in the BFRS internal fiber lap tandem, forming a structurally stable three-dimensional space-bearing structure to inhibit the generation and development of cracks [30,31]. Immediately after the initial cracking of the test block, the fibers across the crack consume energy through fiber debonding slip work to inhibit crack expansion. At this time, the fibers at the crack can continue to bear the load, and through the role of the bridge and the three-dimensional skeleton will be the uniform transfer of stress to inhibit the matrix Shedding, until the fiber gradually debonding fracture failure, making the BFRS toughness enhanced. Fig. 13 shows the pressure diffusion diagram of BFRS.

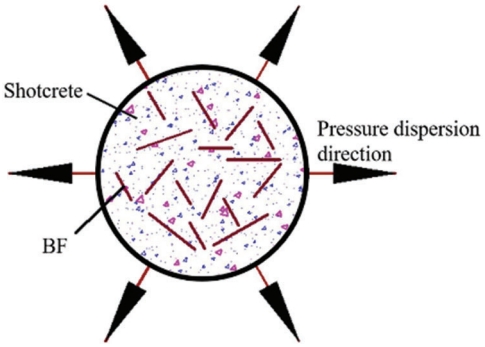

Figure 13: Pressure dispersion diagram of basalt fiber shotcrete

3.2 Results of Orthogonal Experiments

The mechanical property test results of nine groups of HFS-BFRS are shown in Fig. 14. Each factor and its corresponding level are evenly distributed. So the results of each factor level are considered as the average of the same level test, and the statistical results of different factor levels reflect the influence of each variable on the performance of HFS-BFRS.

3.3 Range Analysis

In order to investigate the effects of cement-sand ratio (A), basalt fiber volume fraction (B), and naphthalene-based high-efficiency water-reducing agent (C) on the mechanical properties of concrete, range analysis was conducted on the orthogonal experimental results, as shown in Table 8.

As can be seen from the range values of each factor of test block strength in Table 8, when C/H is between 0.22 and 0.28, FDN is between 1% and 1.5%, and BF Vol is between 0.05% and 0.15%: 1) FDN has a great influence on 3 d compressive strength, R is 3.8 MPa, followed by C/H, R is 3.5 MPa, and BF Vol, R is 2.1 MPa. The main and secondary influencing factors of 28 d compressive strength are C/H > FDN > BF Vol, R is 7.1, 2.9, 2.8 MPa, respectively, which has a greater advantage on 28 d compressive strength C/H. 2) The main influencing factor of 3 d splitting tensile strength is FDN, followed by BF Vol, C/H, and R is 0.7, 0.5, and 0.4 MPa, respectively. BF Vol has the greatest influence on 28 d splitting tensile strength, and R is 0.8 MPa, while FDN and C/H have little influence, and R is 0.4 and 0.2 MPa. 3) 3 d flexural strength is significantly affected by FDN and BF Vol, while C/H has little effect. The flexural strength of 28 d was most significantly affected by C/H.

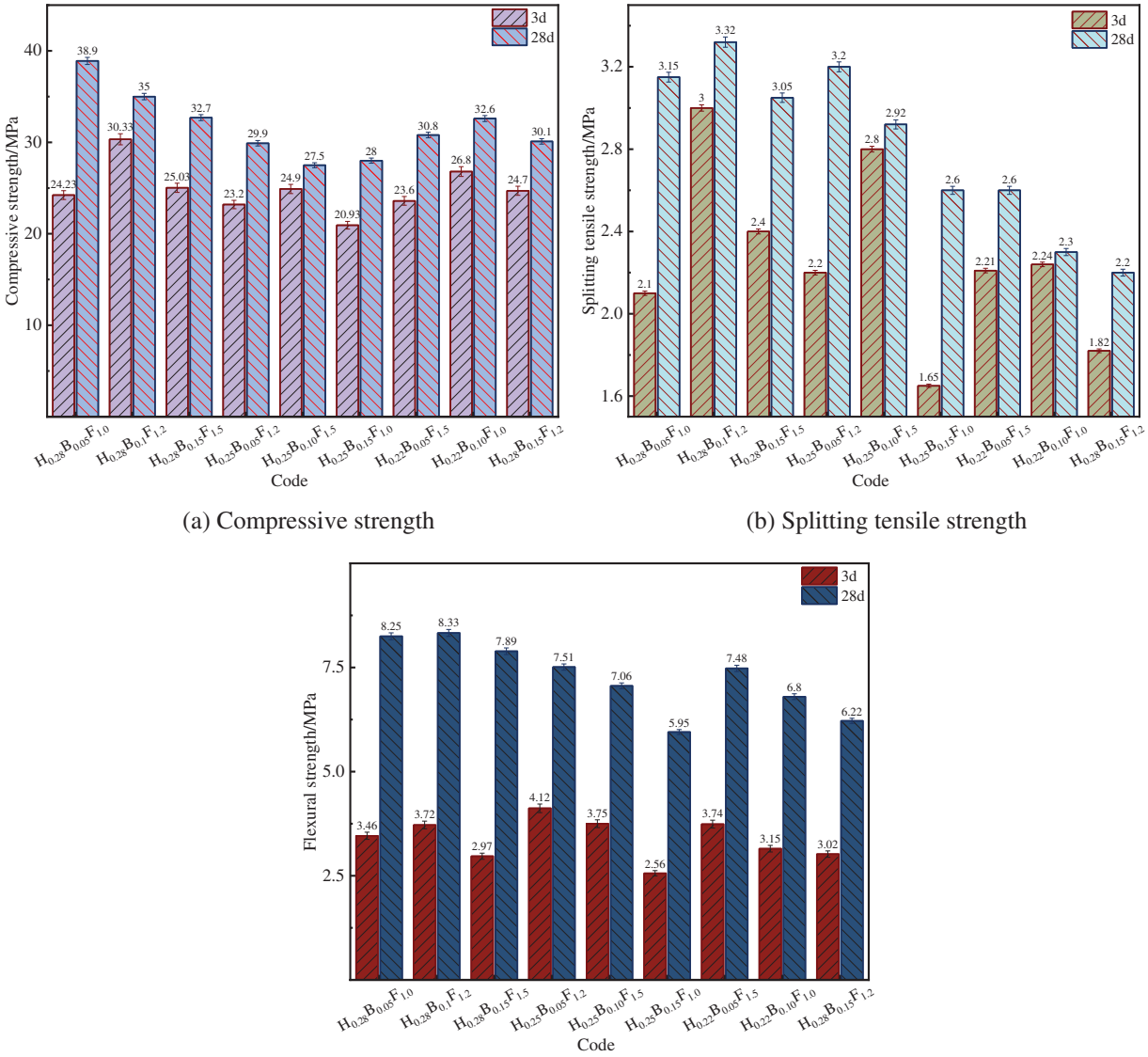

(a) Compressive strength

(b) Splitting tensile strength

(c) Flexural strength

Figure 14: Orthogonal test results

Table 8: Range analysis

Index	Age	Factors	K1	K2	K3	k1	k2	k3	R
Compressive strength/f_{cu}/MPa	3 d	A	69.00	79.60	75.10	23.0	26.5	25.0	3.5
		B	71.96	78.23	73.53	24.0	26.1	24.5	2.1
		C	71.03	82.03	70.66	23.7	27.3	23.6	3.8
	28 d	A	85.40	106.6	93.50	28.5	35.5	31.2	7.1
		B	99.50	95.00	91.00	33.2	31.7	30.3	2.8
		C	99.60	95.10	90.80	33.2	31.7	30.3	2.9

(Continued)

Table 8 (continued)

Index	Age	Factors	K1	K2	K3	k1	k2	k3	R
Splitting tensile strength/f_{ts}/MPa	3 d	A	7.500	6.650	6.27	2.50	2.20	2.10	0.4
		B	5.990	7.020	7.410	2.00	2.30	2.50	0.5
		C	6.510	8.040	5.870	2.20	2.70	2.00	0.7
	28 d	A	8.050	8.720	8.570	2.70	2.90	2.90	0.2
		B	9.520	8.720	7.100	3.20	2.90	2.40	0.8
		C	8.950	8.540	7.850	3.00	2.80	2.60	0.4
Flexural strength/f_{cf}/MPa	3 d	A	10.15	10.43	9.910	3.40	3.50	3.30	0.2
		B	9.17	10.86	10.46	3.10	3.60	3.50	0.5
		C	11.32	10.62	8.550	3.80	3.50	2.90	0.9
	28 d	A	24.47	20.52	20.50	8.20	6.80	6.80	1.4
		B	21.00	22.06	22.43	7.00	7.40	7.50	0.5
		C	23.24	22.19	20.06	7.70	7.40	6.70	1.0

3.4 Analysis of Variance

The idea of range analysis is simple and clear, but it has limitations, and it is impossible to distinguish the experimental results caused by different factor levels or test errors. In this study, the statistical analysis software SPSS was used to conduct ANOVA on the experimental results, and the significant results are shown in Table 9.

Table 9: Analysis of variance

Index	Age/d	Factors	SS_J	Df	MS	F	P	Significance
Compressive strength/f_{cu}/MPa	3	A	18.70	2	9.400	66.60	0.015	*
		B	7.100	2	3.500	25.20	0.038	*
		C	27.80	2	13.90	99.00	0.010	**
	28	A	76.30	2	38.10	62.80	0.016	*
		B	12.10	2	6.100	9.900	0.092	
		C	13.00	2	6.500	10.60	0.086	
Splitting tensile strength/f_{ts}/MPa	3	A	0.264	2	0.132	69.18	0.014	*
		B	0.359	2	0.179	93.88	0.011	*
		C	0.829	2	0.414	216.8	0.005	**
	28	A	0.082	2	0.041	5.230	0.160	
		B	1.013	2	0.507	64.32	0.015	*
		C	0.206	2	0.103	13.08	0.071	
Flexural strength/f_{cf}/MPa	3	A	0.045	2	0.023	4.390	0.186	
		B	0.520	2	0.260	50.50	0.019	*
		C	1.380	2	0.692	134.4	0.007	**
	28	A	3.500	2	1.740	45.10	0.022	*

(Continued)

Table 9 (continued)

Index	Age/d	Factors	SS_J	Df	MS	F	P	Significance
		B	0.367	2	0.180	4.750	0.174	
		C	1.750	2	0.880	22.65	0.042	*

According to the *P* values in Table 9, it can be concluded that: 1) FDN has a highly significant influence on 3 d compressive and splitting tensile strength, and C/H and BF Vol are significant influences. In the 28 d compressive strength, only C/H has a significant effect, and the other effects are not significant. In the 28 d tensile strength, only BF Vol is significant, which is consistent with the range analysis results. 2) 3 d flexural strength is most significantly affected by FDN, followed by BF Vol, while C/H has no significant effect. The 28 d flexural strength was significantly affected by C/H and FDN but not by BF Vol, which was consistent with the range analysis results.

3.5 Analysis of Factor Indicators

To analyze the relationship between factors and mechanical property indexes, the corresponding k values of each factor (k1, k2, k3) were taken as the ordinate, and the level of each factor was taken as the abscissa to make the relationship trend chart between factors and indexes, as shown in Fig. 15.

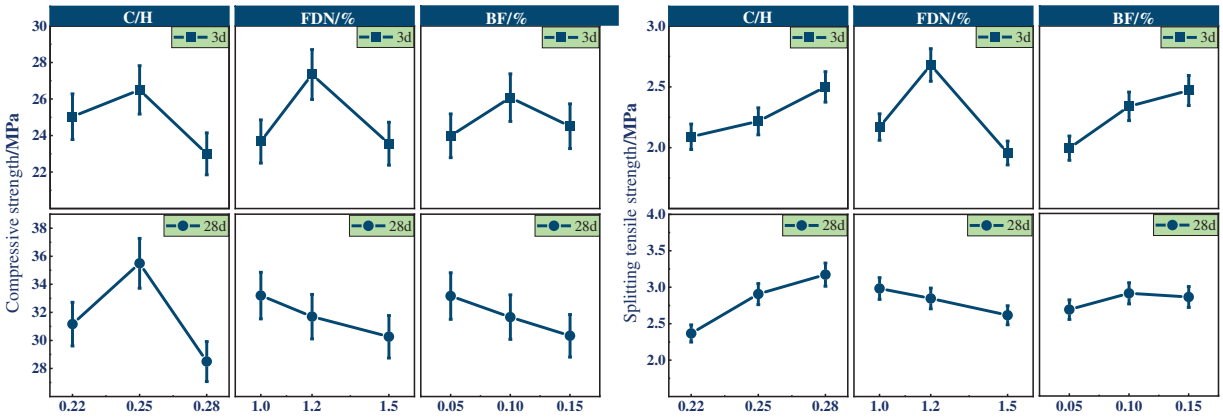

(a) Uniaxial compression

(b) Splitting tensile strength

(c) Flexural strength

Figure 15: Trend chart of factor indicators

3.5.1 Compressive Strength Analysis

Fig. 15a shows that the 3 and 28 d compressive strengths first increase and then decrease with the increase of C/H, indicating that the optimal strengthening effect of C/H is not simply linear with the dosage. HFS fine powder can optimize the particle size of cementitious materials to improve the compacting degree of the system [32]. When it exceeds a certain limit, the physical filling effect of fine powder particles on the particle size optimization of cementitious materials is smaller than its dilution effect, which leads to the weakening of the skeleton function of sand particles and the difficulty in maintaining the strength improvement. When C/H is 0.25, the strength reaches its best. In addition, the influence trend of FDN and BF Vol on 3 d compressive strength is similar, which increases first and then decreases. For 28 d compressive strength, FDN and BF Vol are linearly and negatively correlated with each other. According to range analysis, the extreme values of the two are 2.9 and 2.8, respectively, which are relatively small. The optimal combination of early and late compressive strength at a given level is $H_{0.25}B_{0.10}F_{1.2}$.

3.5.2 Splitting Tensile Strength Analysis

Fig. 15b shows the changing trend of splitting tensile strength. Since BF Vol and C/H are significant influencing factors on the early tensile strength, they show a positive correlation trend on the early and late tensile strength. When BF Vol is 0.15% and C/H is 0.28, the tensile strength reaches the maximum, the 3 d tensile strength increases by 24% and 19%, and the 28 d tensile strength increases by 8% and 34%, respectively. The increase of C/H is conducive to the improvement of its gradation, thus reducing the amount of free water in concrete and the leakage of water enriched on the sand surface in concrete, resulting in the reduction of the thickness of the interfacial transition zone and the enhancement of the splitting tensile strength [33]. With the addition of BF, the generation and development of micro-cracks in the concrete matrix are effectively suppressed, the stress concentration of the crack tip is delayed, the ultimate stress time of concrete is delayed, and the splitting tensile strength is improved. With the increase of FDN content, the early tensile strength first increased and then decreased, reaching the peak value when FDN was 1.2%. According to range analysis and variance analysis, the extreme value of FDN for the late tensile strength was 0.4 MPa, which was not a significant influencing factor. The optimal combination of tensile strength is $H_{0.28}B_{0.15}F_{1.2}$.

3.5.3 Flexural Strength Analysis

Fig. 15c shows the changing trend of flexural strength. Combined with Table 8, it can be seen that the extreme value of C/H on the early flexural strength is 0.2 MPa, and the curve in the trend chart is relatively gentle. Table 9 shows that C/H has no significant influence on the early flexural strength, while for the later flexural strength, the strength value gradually increases with the increase of C/H, and reaches the maximum when C/H is 0.28. When the FDN increased from 1% to 1.5%, the early and late flexural strength decreased by 14% and 24%, respectively. When BF Vol is increased from 0.05% to 0.15%, the early and late flexural strength can be increased by 15.7% and 6.7%, respectively. Therefore, the optimal combination of flexural strength is $H_{0.28}B_{0.15}F_{1.0}$.

4 Spray Test

Carry out on-site spraying experiments with a small shotcrete truck of the enterprise. See Table 10 for the mixed proportion of the spraying test. The size of the injection mold is 460 mm × 460 mm × 120 mm. The air pressure of the jet is controlled at about 0.25 MPa. The water pressure at the nozzle is controlled at about 1 MPa, and the distance between the nozzle and the template is kept at 1 m. And the nozzle is perpendicular to the surface of the template, after spraying, it is covered with plastic film, and the spraying process is shown in Fig. 16. Cutting after 28 d of maintenance of the large plate, the cutting size is 100 mm × 100 mm × 100 mm.

Table 10: Injection test mix ratio

Cement/kg/m³	Water/kg/m³	HFS/kg/m³	FDN/kg/m³	BF/kg/m³	AC/kg/m³
440	220	1760	5.28	2.7	8.8

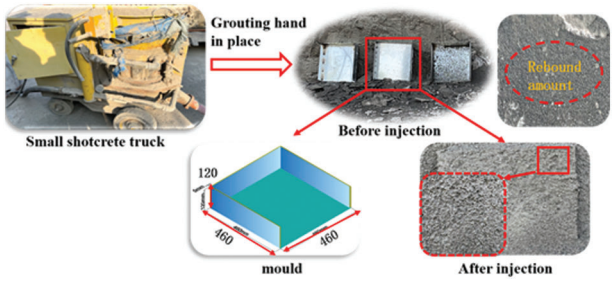

Figure 16: Field injection test diagram

The spring back rate of the injection test was calculated to be about 8.9%. The slurry fluidity was good during the injection process, and there was no pipe-blocking phenomenon. The strength test of the cut cube test block met the design requirements.

5 Conclusion

1. The compressive strength of HFS-BFRS increases exponentially at the same age, and decreases linearly with the water binder ratio and accelerator dosage. A fitting equation for the growth characteristics of HFS-BFRS compressive strength is proposed with the water binder ratio, accelerator dosage, and age as variables.
2. The addition of Naphthalene high-efficiency water-reducing agent makes up for the deficiency of the working performance of HFS-BFRS, the cohesion and water retention of HFS-BFRS are improved, and the slump can be increased by up to 139%, which not only ensures the mechanical properties of HFS-BFRS but also guarantees its pump-ability and ejection ability.
3. The 3 d strength of HFS-BFRS is greatly affected by FDN, and the strength of HFS-BFRS is mainly affected by C/H when the age reaches 28 d. Specific performance: 3 d splitting tensile strength, flexural strength, FDN > BF > C/H, 3 d pressure resistance, FDN > C/H > BF. 28 d compressive and flexural strength, C/H > FDN > BF, 28 d splitting tensile strength, BF > FDN > C/H.
4. C/H, FDN and BF have significant effects on 3 d compressive strength. When the age reaches 28 d, only C/H is a significant influencing factor, and the optimal ratio is recommended as $H_{0.25}B_{0.10}F_{1.2}$. BF was the significant influencing factor of splitting tensile strength, and the recommended optimal ratio was $H_{0.25}B_{0.10}F_{1.2}$. The significant influencing factor of bending strength was FDN, and the optimal mixing ratio was $H_{0.28}B_{0.15}F_{1.0}$.
5. C/H and compressive strength are not a simple linear relationship, and there will be a limit between the two, beyond which the strength will be weakened. Secondly, BF can improve the three strengths to a certain extent, and the splitting tensile strength is the most obvious increase, up to 24%. At this time, its dosage is 4.07 kg/m³.
6. Through indoor and field tests, the shotcrete prepared with high silt content as fine aggregate and basalt fiber is feasible, which greatly improves the utilization value of high silt content and can provide a reference for similar problems in the future.

Funding Statement: This work was supported by the National Natural Science Foundation of China (51834001, 52104129), a project supported by the China Postdoctoral Science Foundation (2020M672226, 2022T150195), Key Laboratory of Mine Ecological Effects and Systematic Restoration, Ministry of Natural Resources, Open Fund (MEER-2022-09).

Conflicts of Interest: The authors declare that they have no conflicts of interest to report regarding the present study.

References

1. Wang, D., Shi, C., Farzadnia, N., Shi, Z., Jia, H. (2018). A review on effects of limestone powder on the properties of concrete. *Construction and Building Materials, 192,* 153–166. https://doi.org/10.1016/j.conbuildmat.2018.10.119
2. Fang, H., Yang, J., Song, Y., Huang, W., Chen, J. (2020). Simulation and experimental study on the stone powder separator of a vertical shaft impact crusher. *Advanced Powde Technology, 31(3),* 1013–1022. https://doi.org/10.1016/j.apt.2019.12.035
3. Rayed, A., Omrane, B., Chokri, S., Mohamed Amine, K. (2019). Effects of incorporation of marble powder obtained by recycling waste sludge and limestone powder on rheology, compressive strength, and durability of self-compacting concrete. *Advances in Materials Science and Engineering, 2019,* 4609353. https://doi.org/10.1155/2019/4609353
4. He, H., Wang, Y. L., Wang, J. J. (2020). Compactness and hardened properties of machine-made sand mortar with aggregate micro fines. *Construction and Building Materials, 250,* 118828. https://doi.org/10.1016/j.conbuildmat.2020.118828.
5. Knop, Y., Peled, A., Cohen, R. (2014). Influences of limestone particle size distributions and contents on blended cement properties. *Construction and Building Materials, 71,* 26–34. https://doi.org/10.1016/j.conbuildmat.2014.08.004
6. Shen, W. G., Wu, J. L., Du, X. J., Li, Z. T., Wu, D. et al. (2022). Cleaner production of high-quality manufactured sand and ecological utilization of recycled stone powder in concrete. *Journal of Cleaner Production, 375,* 134146. https://doi.org/10.1016/j.jclepro.2022.134146
7. Wang, X. H., Zhan, Q. Q., Chen, H., Zhang, Y. S., Zhang, J. H. (2022). The influence of stone powder content on the strength and frost resistance of machine-made sand concrete. *Journal of Hefei University of Technology (Natural Science Edition), 45(4),* 500–504+525.
8. Westerholm, M., Lagerblad, B., Silfwerbrand, J., Forssberg, E. (2008). Influence of fine aggregate characteristics on the rheological properties of mortars. *Cement and Concrete Composites, 30(4),* 274–282. https://doi.org/10.1016/j.cemconcomp.2007.08.008
9. Schmidt, M., Harr, K., Boeing, R. (1993). Blended cement according to ENV 197 and experiences in Germany. *Cement, Concrete and Aggregates, 45(2)*.
10. Moir, G. K., Kelham, S. (1997). Developments in the manufacturing and use of portland limestone cement. *Proceedings of Third CANMET/ACI International Conference. American Concrete Institute (ACI)*, pp. 172–142.
11. Aliabdo, A. A., Abd Elmoaty, A. E. M., Auda, E. M. (2013). Re-use of waste marble dust in the production of cement and concrete. *Construction and Building Materials, 50,* 28–41. https://doi.org/10.1016/j.conbuildmat.2013.09.005
12. Rodrigues, D. F., Pan, X. Y., Gencturk, B., Alnaggar, M., Sohail, M. G. et al. (2023). Numerical simulation of the fracture and compression response of self-healing concrete containing engineered aggregates. *Cement and Concrete Composites, 136,* 104858. https://doi.org/10.1016/j.cemconcomp.2022.104858
13. Kizilkanat, A. B., Kabay, N., Akyüncü, V., Chowdhury, S., Akça, A. H. (2015). Mechanical properties and fracture behavior of basalt and glass fiber reinforced concrete: An experimental study. *Construction and Building Materials, 100,* 218–224. https://doi.org/10.1016/j.conbuildmat.2015.10.006

14. Deng, Y. G., Zhao, B. J., Dai, T. T., Li, G. Q., Li, Y. (2022). Study on the dispersibility of modified basalt fiber and its influence on the mechanical properties of concrete. *Construction and Building Materials, 350,* 128839. https://doi.org/10.1016/j.conbuildmat.2022.128839
15. Wang, Y. M., Hu, S. W., Sun, X. P. (2022). Experimental investigation on the elastic modulus and fracture properties of basalt fiber–reinforced fly ash geopolymer concrete. *Construction and Building Materials, 338,* 127570. https://doi.org/10.1016/j.conbuildmat.2022.127570
16. Cakir, F. (2021). Evaluation of mechanical properties of chopped glass/basalt fibers reinforced polymer mortars. *Case Studies in Construction Materials, 15,* e00612. https://doi.org/10.1016/j.cscm.2021.e00612
17. Song, S., Li, X. L., Wang, Z., Wang, W. M. (2022). Orthogonal experimental and theoretical study on mechanical properties of fiber-reinforced recycled powder concrete. *Case Studies in Construction Materials, 17,* e01546. https://doi.org/10.1016/j.cscm.2022.e01546
18. Sim, J., Park, C., Moon, D. Y. (2005). Characteristics of basalt fiber as a strengthing material for concrete structures. *Composites Part B, 36(6),* 504–512. https://doi.org/10.1016/j.compositesb.2005.02.002
19. Dias, D. P., Thaumaturgo, C. (2005). Fracture toughness of geopolymeric concretes reinforced with basalt fibers. *Cement & Concrete Composites, 27(1),* 49–54. https://doi.org/10.1016/j.cemconcomp.2004.02.044
20. Jiao, H. Z., Zhang, W. X., Yang, Y. X., Chen, X. M., Yang, L. H. (2023). Static mechanical characteristics and meso-damage evolution characteristics of layered backfill under the condition of inclined interface. *Construction and Building Materials, 336,* 130113. https://doi.org/10.1016/j.conbuildmat.2022.130113
21. Abbas, Y. M., Iqbal Khan, M. (2016). Fiber–matrix interactions in fiber-reinforced concrete: A review. *Arabian Journal for Science and Engineering, 41(4),* 1183–1198. https://doi.org/10.1007/s13369-016-2099-1
22. Wang, J., Zhan, L. F., Zhang, Y. L. (2022). Analysis of mechanical properties of high-performance shotcrete. *Journal of Jilin Jianzhu University, 39(3),* 47–51.
23. Cusson, D., Hoogeveen, T. (2008). Internal curing of high-performance concrete with pre-soaked fine lightweight aggregate for prevention of autogenous shrinkage cracking. *Cement and Concrete Research, 38(6),* 757–765. https://doi.org/10.1016/j.cemconres.2008.02.001
24. Shi, J. Y., Tan, J. X., Liu, B. J., Chen, J. Z., Dai, J. D. (2021). Experimental study on full-volume slag alkali-activated mortars: Air-cooled blast furnace slag versus machine-made sand as fine aggregates. *Journal of Hazardous Materials, 403,* 123983. https://doi.org/10.1016/j.jhazmat.2020.123983
25. Li, P. L., Yue, L., Ma, H., Yang, X. Y. (2022). Research on influencing factors and growth characteristics of shotcrete strength. *Journal of Guangxi University (Natural Science Edition), 47(5),* 1174–1183. https://doi.org/10.13624/j.cnki.issn.1001-7445.2022.1174
26. He, X. Y., Zheng, Z. Q., Yang, J., Su, Y., Wang, T. W. et al. (2020). Feasibility of incorporating autoclaved aerated concrete waste for cement replacement in sustainable building materials. *Journal of Cleaner Production, 250,* 119455. https://doi.org/10.1016/j.jclepro.2019.119455
27. Cepuritis, R., Wigum, B. J., Garboczi, E. J. (2014). Filler from crushed aggregate for concrete: Pore structure, specific surface, particle shape and size distribution. *Cement and Concrete Composites, 54,* 2–16. https://doi.org/10.1016/j.cemconcomp.2014.03.010
28. Zieliński, K., Olszewski, P. (2005). The impact of basaltic fibre on selected physical and mechanical properties of cement mortar. *Betonwerk und Fertigteil-Technik/Concrete Precasting Plant and Technology, 71(3),* 28–33.
29. Li, X. D., Meng, Q., Wang, W. H., Wang, Q. T. (2019). Effects of basalt fiber admixture amount and admixture method on compressive strength and damage morphology of concrete. *Concrete and Cement Products, 4,* 55–58.
30. Chen, F., Chen, X. (2014). Orthogonal experimental research on strength of concrete reinforced by basalt fiber. *Journal of Fuzhou University (Natural Science Edition), 42(1),* 134–137.
31. Yang, J., Zeng, J. Y., He, X. Y., Hu, H. C., Su, Y. et al. (2021). Eco-friendly UHPC prepared from high volume wet-grinded ultrafine GGBS slurry. *Construction and Building Materials, 308,* 125057. https://doi.org/10.1016/j.conbuildmat.2021.125057

32. Kim, J., Na, S., Zhang, W. (2017). Effect of limestone powder and gypsum on the compressive strength mixture design of blast furnace slag blended cement mortar. *Journal of Advanced Concrete Technology, 15(2),* 67–80. https://doi.org/10.3151/jact.15.67
33. Zhang, L. Q., Chen, Q., Huang, X., Li, B. X. (2020). Effect of stone powder content on properties of C50 granite machine-made sand concrete. *Silicate Bulletin, 39(7),* 2154–2158+2177. https://doi.org/10.16552/j.cnki.issn1001-1625.2020.07.019